Long-Lived Magnetization in an Atomic Spin Chain Tuned to a Diabolic Point

Elbertse, R.J.G.; Borodin, D.; Oh, J.; Ahn, T.; Hwang, J.; Rietveld, J.C.; Heinrich, A.J.; Delgado, F.; Otte, S.; Bae, Y.

DOI
10.1103/PhysRevLett.133.166703

Publication date
2024

Document Version
Final published version

Published in
Physical review letters

Editors' Suggestion | Featured in Physics

Long-Lived Magnetization in an Atomic Spin Chain Tuned to a Diabolic Point

R. J. G. Elbertse,[1] D. Borodin,[2] J. Oh,[2,3] T. Ahn,[2,3] J. Hwang,[2,3] J. C. Rietveld,[1] A. J. Heinrich,[2,3] F. Delgado,[4,*] S. Otte,[1,†] and Y. Bae[2,3,‡]

[1]*Department of Quantum Nanoscience, Kavli Institute of Nanoscience, Delft University of Technology, Delft, The Netherlands*

[2]*Center for Quantum Nanoscience, Institute for Basic Science (IBS), Seoul, South Korea*

[3]*Department of Physics, EWHA Womans University, Seoul, South Korea*

[4]*Instituto Universitario de Estudios Avanzados IUDEA, Departamento de Física, Universidad de La Laguna, La Laguna, Tenerife, Spain*

(Received 11 April 2024; revised 2 July 2024; accepted 14 August 2024; published 15 October 2024)

Scaling magnets down to where quantum size effects become prominent triggers quantum tunneling of magnetization (QTM), profoundly influencing magnetization dynamics. Measuring magnetization switching in an Fe atomic chain under a carefully tuned transverse magnetic field, we observe a nonmonotonic variation of magnetization lifetimes around a level crossing, known as the diabolic point (DP). Near DPs, local environment effects causing QTM are efficiently suppressed, enhancing lifetimes by three orders of magnitude. Adjusting interatomic interactions further facilitates multiple DPs. Our Letter provides a deeper understanding of quantum dynamics near DPs and enhances our ability to engineer a quantum magnet.

DOI: 10.1103/PhysRevLett.133.166703

In quantum mechanical systems, unusual dynamic processes occur when energy levels approach and mix with each other. In a two-parameter space, the degeneracy between orthogonal states creates a level crossing of energy surfaces (Fig. 1(a)), the shape of which reminds of the toy, *diabolo*, and thus is dubbed a diabolic point (DP) [1]. This DP has attracted significant attention in quantum magnets [2], which are characterized by two metastable magnetization states separated by an energy barrier [3,4]. In the vicinity of the DP, quantum tunneling of magnetization (QTM) between these states is suppressed due to destructive interference among separate tunneling paths [5–7]. While the importance of DPs has been shown from ensembles of molecular magnets [2,8,9] and in quantum dot systems [10], precise control of local environments as a control knob of DPs has remained elusive.

Manipulation of magnetic atoms with a scanning tunneling microscope (STM) allows for the assembly of prototypical quantum magnets with controllable energy barriers ranging from 100 μeV to 100 meV [11–13]. The lifetime of magnetization states in these magnets can be determined by monitoring the spin-polarized current through one of the magnet's atoms over time [14]. When the magnetic anisotropy barrier exceeds the thermal energy, the lifetime is dominated by through-the-barrier transitions, i.e., QTM, resulting from hybridization between quantum states on either side of the barrier. While various systems have been studied with different degrees of spin state hybridization [14] and spin-spin interactions [14,15], it remains challenging to vary individual parameters due to the discrete nature of binding sites on surfaces. Instead, a more effective control knob for QTM may be achieved by exploiting the physics of a DP, where the hybridization of the quantum states is expected to quench, allowing, at least in principle, arbitrarily long lifetimes.

In this Letter, we demonstrate the manifestation of DPs through the spin dynamics of nanomagnets by assembling Fe atoms into chains on $Cu_2N/Cu(100)$ using an STM operating at ~1.3 K [16]. Precisely adjusting chain length and interatomic spacing enables us to tailor the spin-spin interactions and thereby to engineer DPs in a controlled manner (see Supplemental Material Note 1 and reference [17] therein). When tuning the direction and strength of the external magnetic field near a DP, we observed a significant increase of magnetization lifetimes, with

*Contact author: fdelgadoa@ull.edu.es

†Contact author: a.f.otte@tudelft.nl

‡Contact author: bae.yujeong@qns.science

Present address: Empa, Swiss Federal Laboratories for Materials Science and Technology, nanotech@surfaces Laboratory, Switzerland.

enhancement of up to 3 orders of magnitude. We provide a comprehensive picture of the quantum state composition near the DP, offering a rational strategy to control the spin dynamics of quantum magnets.

To model a chain of N Fe atoms on Cu sites of Cu_2N, we consider a spin Hamiltonian that includes the Zeeman energy, the uniaxial and transverse magnetic anisotropy terms for each atom, as well as the Heisenberg exchange interaction between neighboring atoms [14,18–20]:

$$H = \sum_{i}^{N} [g_i \mu_B \boldsymbol{B}_i^{\mathrm{tot}} \cdot \boldsymbol{S}_i + D_i S_{i,z}^2 + E_i (S_{i,x}^2 - S_{i,y}^2)] + \sum_{i}^{N-1} J_i \boldsymbol{S}_i \cdot \boldsymbol{S}_{i+1}. \quad (1)$$

For an Fe atom on site i, $\boldsymbol{B}_i^{\mathrm{tot}} = \boldsymbol{B} + \boldsymbol{B}_i^{\mathrm{tip}}$ is the total magnetic field composed of external and tip fields, μ_B the Bohr magneton, and $\boldsymbol{S}_i$ the spin operator with a magnitude of $S_i = 2$. Note that we allow for subtle variations in the values of the g factor g_i, anisotropy parameters D_i and E_i, and exchange interaction strength J_i between atoms in the chain, since these parameters might vary due to subtle changes in the local strain in the underlying Cu_2N layer, as evidenced by variations of Hamiltonian parameters throughout the literature (see Supplemental Material Note 2 [21] and references [22–31] therein). The easy-axis z is oriented along the in-plane Cu—N bonds [11]; we define the x and y axes as the remaining in-plane direction and the out-of-plane direction, respectively [Fig. 1(b)]. Since the chain is not perfectly aligned with the external magnetic field in the experiment, the angle α is used to decompose the magnetic field into both transverse (B_x) and longitudinal (B_z) components.

We investigate the DPs as a function of the transverse magnetic field, B_x. Solving the spin Hamiltonian [Eq. (1)] for a single Fe atom ($N = 1$) gives the analytical solution for the $B_{x,n}$ fields where the DPs appear [32,33]:

$$B_{x,n} = \frac{n\sqrt{2E(E-D)}}{g\mu_B}. \quad (2)$$

Here, n is the diabolic point index that ranges from $2S - 1$ to $1 - 2S$ in double-integer steps. To estimate the location of DPs, we use Hamiltonian parameters which have been obtained from previous works, see Supplemental Material Note 2 [21]. For a single Fe atom at the Cu site, the lowest positive magnetic field DP ($n = 1$) is expected at $B_{x,1} \approx 9.5$ T. A second DP ($n = 3$) can be reached at even larger values of B_x. As depicted in Fig. 1(a), when $B_x = B_{x,1}$ and $B_z = 0$, an energy level crossing occurs between the two lowest-lying eigenstates, ψ_0 and ψ_1. When a small B_z is applied, sweeping B_x results in an avoided level crossing, as shown by the surface cut in Fig. 1(a).

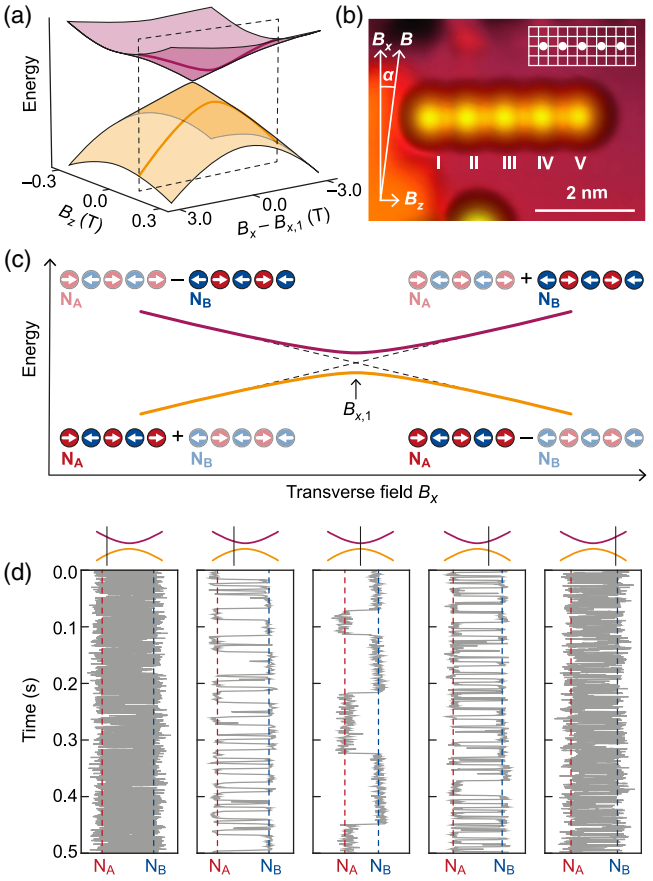

FIG. 1. Diabolic points in Fe atomic chains on Cu_2N. (a) Energy levels for the two lowest-lying states of a single Fe atom (orange for the ground state ψ_0 and pink for the first-excited state ψ_1) with a diabolic point at the crossing. Thick lines show a cut of the energy surfaces, indicating the corresponding energies of the two states at a finite B_z outlined by the dashed rectangle. Note that the scale for the z component of the magnetic field is 1 order lower than that of the x component. (b) Constant-current STM image of an antiferromagnetic Fe_5 chain ($V_{DC} = 100$ mV, $I = 10$ pA, $B = 2$ T, $T = 1.3$ K). Atoms are labeled in Roman numerals (I–V). Schematics shows Fe atoms (white circles) on top of Cu_2N lattice. The intersections of grid lines correspond to the nitrogen atom position in Cu_2N. Magnetic field directions are tilted by the angle $\alpha \approx 0.2°$ with respect to the crystal axis. (c) Schematic overview of state composition for ψ_0 and ψ_1 of Fe_5 along a similar cut as in panel a. (d) Current traces taken for atom III in the Fe_5 chain at different magnetic fields around the DP, located at 4.1 T, as indicated in the schematics above ($V_{DC} = 3$ mV, $I \sim 10$ pA, $T = 1.3$ K).

Diabolic points in atomic chains of length $N > 1$ with $|J/D| \lesssim 1$ can be understood in a similar fashion, although there are now N DPs for each DP index, leading to a total of $2NS$ DPs. Now, the spin-spin interaction between the atoms can be used as a control knob for the location of DPs as a function of B_x. By adjusting the number of atoms in the chain and their interaction, we are able to precisely determine the magnetic field values at which DPs are

expected to occur (see Supplemental Material Note 3 [21] and references [34,35] therein).

The magnetic fields needed to identify a DP in a single Fe atom are beyond the available transverse magnetic field (6 T) of our instrument [11,33]. However, for longer chains, the DP eventually becomes accessible within the range of our experimental capabilities. Our initial calculations using Eq. (1) predicted a DP for an antiferromagnetically coupled Fe_5 chain [Fig. 1(b)] at $B_{x,1} \sim 4$ T (see Supplemental Material Note 3 [21]), which guided our magnetization lifetime measurements.

Figure 1(c) schematically shows the energy levels of the two lowest-lying states (ψ_0 and ψ_1) in the antiferomagnetic Fe_5 chain as a function of transverse magnetic field. For $B_x \ll B_{x,1}$, these two states are mainly composed of Néel states, denoted as $N_A = \{-2, +2, -2, +2, -2\}$ and $N_B = \{+2, -2, +2, -2, +2\}$ (expressed in the S_z basis), with subtle contributions from other spin states. Owing to the presence of a finite longitudinal component of the field and N being an odd number, the ground state ψ_0 has a larger contribution from N_A ($> 98\%$) compared to N_B, while the opposite holds for ψ_1. The finite contributions of both N_A and N_B in these two states demonstrate that the Néel states are hybridized, enabling QTM between them. In ψ_0, the contributions of N_A and N_B are symmetric, whereas in ψ_1 they are antisymmetric. Around $B_x = B_{x,1}$, the two states undergo an avoided level crossing, beyond which their symmetry is inverted. At the DP, the contribution of the minority Néel state vanishes, significantly enhancing the purity of ψ_0 and ψ_1 as mainly composed of N_A and N_B, respectively, thereby suppressing QTM.

Using spin-polarized STM, we investigate the influence of DPs on the magnetization of Fe atomic chains by capturing the time-dependent magnetization switching of the Fe chain at different B_x. By positioning the tip above one of the Fe atoms in the chain, we observe telegraph noise in the current signals, arising from the magnetization switching between the two lowest-lying states of the chain [Fig. 1(d)]. The specific spin polarization of the tip, and which atom in the chain is being probed, determines the current value characteristic for N_A and N_B. Note that the magnetization of the STM tip may not be fully aligned with the external magnetic field direction [36–38], which enables the detection of the longitudinal component of the chain magnetization as a function of the transverse magnetic field. For $B_x \ll B_{x,1}$, we detect rapid, yet clearly distinguishable switching events between two distinct current values. As B_x approaches the DP, the switching rate markedly decreases, to gradually increase again beyond the DP.

To quantitatively investigate the evolution of spin dynamics around the DPs, we extract the values of magnetization lifetimes from a current trace as demonstrated in Fig. 2(a). Shown are the lifetimes τ_A and τ_B, representing the duration between consecutive switches in

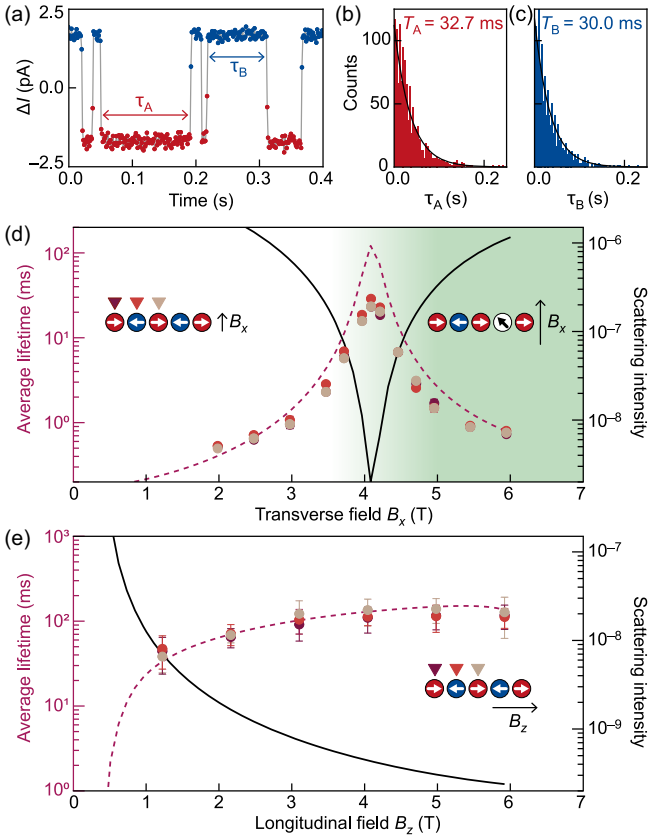

FIG. 2. Lifetime of magnetization states of antiferromagnetic Fe_5 chains at different magnetic fields. (a) A current trace obtained at a constant tip height on atom III of the Fe_5 chain near the diabolic point ($B_x \approx 4$ T). The magnetoresistive tunnel current recorded with a spin-polarized tip reveals switching between two magnetization states of the chain, dominated by N_A (red) and N_B (blue), respectively. The data was shifted by about 8 pA to center the middle values around zero, mitigating background fluctuations caused by drift. (b),(c) Histograms of lifetimes τ_A and τ_B, as defined in (a), with a fit to an exponential function to determine lifetimes T_A and T_B, respectively. (d) Average lifetimes T_{avg} measured for atoms I, II, and III of an antiferromagnetic Fe_5 chain at different B_x. Different colors of data points correspond to the results obtained from different atoms, see diagram. The corresponding longitudinal component B_z is approximately 0.35% of the transverse magnetic field, due to a small angle ($\alpha \approx 0.2°$) between the external magnetic field and the crystal axes. The error bars represent 1 standard deviation of the fitting error. The lifetimes and scattering intensities, calculated using master rate equations, are given in the purple dashed and black solid lines, respectively, assuming $T = 3$ K for better agreement with the experimental results (see Table S2 [21] for further details). Background color and diagrams indicate the quanta of S_x in the ground state: zero before the diabolic point and one after the diabolic point, with the diabolic point at $B_{x,1} \approx 4.1$ T. (e) Lifetime obtained similar to (d), but for a magnetic field applied along the longitudinal axis, B_z. The simulation was conducted at 1.3 K. Measurement conditions: $V_{DC} = 3$ mV, $I = 10$ pA, $T = 1.3$ K.

eigenstates dominated by N_A and N_B, respectively. By collecting sufficiently long traces, we obtain histograms for τ_A [Fig. 2(b)] and τ_B [Fig. 2(c)], enabling us to extract characteristic lifetimes T_A and T_B, respectively [14]. Finally, we define $T_{avg} = (T_A^{-1} + T_B^{-1})^{-1}$ as the average lifetime of the magnetization states. The extracted T_{avg} for atoms I–III of the antiferromagnetic Fe_5 chain are shown as a function of the transverse magnetic field in Fig. 2(d), showing a pronounced peak at $B_x = 4.1$ T spanning two orders of magnitude. As we will demonstrate below, we can associate this field value to the first DP of the chain $B_{x,1}$. This DP coincides with a minimum in the scattering amplitude, shown by the black solid line in Fig. 2(d) and defined as $\sum_{a=x,y,z} |\langle\psi_0|S_{a,i}|\psi_1\rangle|^2$, which is an indication of the hybridization between ψ_0 and ψ_1.

Note that, in Figs. 2(b) and 2(c), the characteristic lifetimes T_A and T_B are comparable, indicating negligibly small energy differences between the two states. However, the presence of a small longitudinal field induces an avoided level crossing rather than a level crossing (see Supplemental Material Notes 4 and 7 for further details [21]), due to the extreme sensitivity of the DP to longitudinal magnetic fields. This results in a finite width of the peak in the lifetime, enabling us to measure the DP. This observed trend occurs for all atoms of the chain and is robust to various experimental parameters (see Supplemental Material Note 5 [21]).

The dashed line in Fig. 2(d) represents a simulation of the lifetime measurements of the chain based on master rate equations (see Supplemental Material Note 3 [21]). In our simulation, we did not account for the effects of the x component of the tip field on the lifetime curves, as evidenced by the current dependence of the DPs, where the overall shape of the lifetime curves near the DPs remains intact at different tip fields (see Supplemental Material Note 10 [21] and reference [39] therein). Neither the simulations nor the measurements show a peak reaching infinity, owing to minute contributions of states other than N_A and N_B. The experimental data show slightly lower lifetimes than the simulation, especially close to the DP. We attribute this deviation to accidental high-energy electrons caused by voltage noise, leading to over-the-barrier excitations.

Until now we have described the situation in terms of the S_z basis. However, for interpretation purposes, it is insightful to consider the situation in terms of the S_x basis. For $B_x < 4.1$ T, the expectation value of S_x in the ground state approaches zero, indicated by the white background and the diagram on the left side of Fig. 2(d). The first excited state contains a single quantum of S_x (i.e., $|\langle S_x\rangle| = 1$). Past the DP, i.e., the avoided level crossing, the states are inverted, transferring the finite S_x magnetization to the ground state, as indicated by the green color and the diagram on the right side of Fig. 2(d). Note that the ground state now consists of a superposition of five spin states, each having the quantum of S_x on a different atom.

We also demonstrate that the increase of lifetime through the DP emerges only for this specific orientation of the magnetic field with respect to the quantization axis. When the magnetic field is swept along the easy axis of the antiferromagnetic Fe_5 chain, no peak in the lifetime is observed, see Fig. 2(e). Within the range of available magnetic fields of B_z (up to ~6 T), there is no energy level crossing. The lifetime slightly increases at higher B_z due to a decrease in scattering intensity. This behavior is strictly monotonic and arises from an increasing imbalance in the Néel state contributions in each eigenstate, as indicated by the lifetime imbalances between them (Supplemental Material Note 11 [21]).

The finite energy difference between the two lowest energy states at the avoided level crossing is responsible for the width of the observed peak in Fig. 2(d) and therefore limits the efficiency of increasing magnetization lifetimes. The energy difference at the DP emerges as a consequence of Zeeman energy, resulting from a small angle α between the quantization axis of the Fe atoms with respect to the applied magnetic field. This suggests that in order to achieve a sharper peak, one must achieve a null magnetic field along B_z. This is practically impossible, as α will inevitably be nonzero in our experimental setup. An alternative approach would be to make use of even-length antiferromagnetic chains, where both Néel states have equal energy, irrespective of B_z. In line with this idea, Fig. 3(a) shows magnetization lifetimes measured on an Fe_6 chain, where a sharper peak than on the Fe_5 chain is observed.

The lifetime of the Fe_6 chain increases by nearly 3 orders of magnitude at the DP, which appears at a lower magnetic field compared to the Fe_5 chain. The overall lifetime has also increased, as larger chains are inherently more stable [14]. Despite the expected absence of Zeeman splitting between the two lowest-lying states of the antiferromagnetic Fe_6 chain, the observed peak shows a finite width, indicating broken symmetry between the Néel states. Our analysis (see Supplemental Material Note 6 [21]) suggests that the primary reason of this asymmetry is variations in the g factors of the atoms in the chain. The difference in g factors results in an energy discrepancy of approximately 50 μeV at $B_x \approx 6$ T, favoring one Néel state at higher magnetic fields.

It is noteworthy that this considerable enhancement of lifetime near the DP is only apparent when the magnetization lifetime is primarily determined by the QTM. Once the over-the-barrier transitions become frequent, the magnetization anomaly diminishes, and we only observe a subtle change in lifetime, as shown by the bias dependence of the lifetime curves (see Supplemental Material Note 9 [21]).

Antiferromagnetic Fe atom chains showed one DP in the transverse magnetic field ranging from 0 to 6 T. However, adjusting magnetic interactions between atoms in the chain through atom manipulation gives us the possibility to change

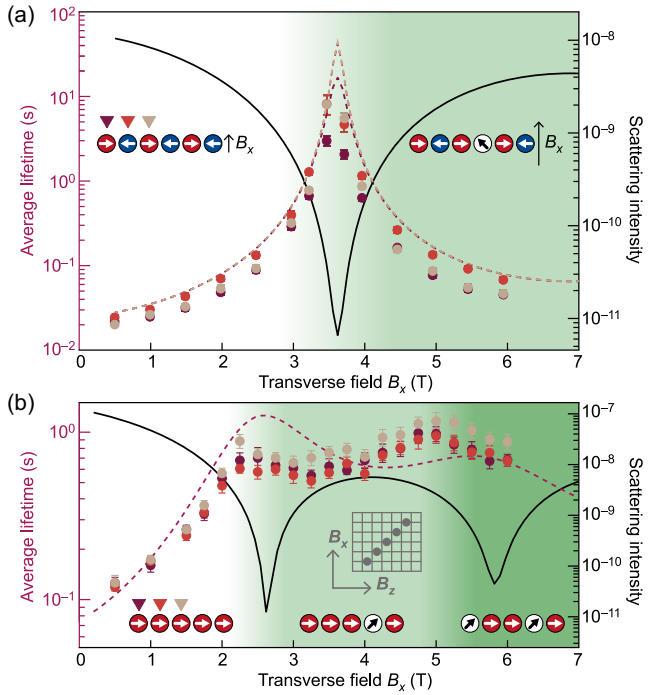

FIG. 3. Tuning diabolic points. (a) Lifetime of an antiferromagnetic Fe_6 chain. Data points were obtained for atoms I–III in the chain, as depicted in the diagram with different colors ($V_{DC} = 3$ mV, $I = 10$ pA, $T = 1.3$ K, $\alpha \approx 5°$). Dashed lines show the calculated lifetimes for each atom using master rate equations. Background color and diagram indicate the quanta of S_x in the ground state, which increases from zero to one upon passing the diabolic point. The solid black line indicates the scattering amplitude from the simulation. (b) Similar to panel a, but for a ferromagnetic Fe_5 chain, and $\alpha \approx 0.2°$. Background color and diagrams indicate a second quantum of S_x entering the ground state as the second diabolic point at around 5 T is passed. Note that the easy axis z and hard axis x are defined along the crystallographic directions, see inset. The error bars represent the fitting errors with 2 standard deviations.

the location and spacing of DPs. Our simulations indicate that a ferromagnetic Fe_5 chain ($J < 0$) is the most likely candidate where multiple DPs can be observed, given the magnetic field range of our experimental setup. In this case, the chain tends to behave as a macrospin with a large total spin. When the coupling is sufficiently strong, this leads to NS positive DPs all equally spaced across the transverse magnetic field. The highest-field DP corresponds to the $B_{x,3}$ value of a single Fe, while the lowest-field DP occurs at $B_{x,3}/(2NS-1)$. Consequently, the DPs for ferromagnetic chains occur at lower magnetic field values.

We built a ferromagnetic Fe_5 chain by placing the 5 atoms diagonally with respect to the easy axis, see inset of Fig. 3(b), leading to $J = -0.7$ meV [15]. Figure 3(b) shows that this chain exhibits two distinct peaks in lifetimes as a function of B_x within our operation range; one at 2.5 T and one at 5.0 T. The second DP is associated with delocalized states where two different atoms in the chain gain a quantum of S_x (i.e., $|\langle S_x \rangle| = 1 \rightarrow 2$). Hence, this may be associated with two-magnon states [40,41].

The simulation results, see the dashed line in Fig. 3(b), qualitatively reproduce the experimental observations but fail to reproduce the exact positions of the DPs. While the scattering intensity does still contain two clearly distinguishable peaks, both the measured and simulated lifetime curves show comparably shallow peaks. We believe that this is due to the overlapping of the two lifetime peaks as well as a larger Zeeman energy associated with the ferromagnetic coupling. The larger energy not only broadens the peaks but also decreases the energy difference between ψ_1 and higher energy states, resulting in more over-the-barrier transitions.

Our Letter presents a comprehensive approach, combining experimental and theoretical methods, to elucidate the physics of magnetization stability of individual atomic spin chains near a DP. We have demonstrated that the switching rate between the two lowest energy levels can be precisely controlled through tailored transverse magnetic fields, which suppresses quantum tunneling of magnetization. This suppression emerges as a consequence of dehybridization of the lowest lying spin states near an avoided level crossing, which, in the case of Fe chains on Cu_2N, results in strong enhancement of lifetimes up to 3 orders of magnitude.

While effects of DPs have been observed previously in single molecule magnets [2,8,9] through ensemble measurements, we showed that DPs in quantum magnets can be manipulated and rationally designed by tailoring the interaction of individual atomic spins on surfaces. The composite nature of atomic spin chains provides the possibility to understand the topology of DPs, with different predicted behavior for ferromagnetic and antiferromagnetic chains, and a crucial role of parity predicted in the latter case.

The dramatic enhancement of the lifetime provides an interesting avenue into spintronics [20,42] and applications of coherent spin dynamics [43,44]. The extreme sensitivity of magnetization lifetimes of a quantum magnet near a DP could be exploited for precise sensing of local and external magnetic fields at the atomic scale. This sensitivity near DPs can also be used to determine parameters of spin Hamiltonians, such as magnetic anisotropy and g factors, with exquisite precision, leading to further understanding of magnetic material in various applications [45–47].

Acknowledgments—R. J. G. E. and S. O. acknowledge support from the Dutch Research Council (NWO Vici Grant VI.C.182.016) and from the European Research Council (ERC Starting Grant No. 676895 "SPINCAD"). D. B., J. O., T. A., J. H., A. J. H., and Y. B. acknowledge support from the Institute for Basic Science (IBS-R027-D1). Y. B. acknowledges support from

Asian Office of Aerospace Research and Development (FA2386-20-1-4052). D. B. acknowledges support from the Alexander von Humboldt Foundation for financial support through a Feodor-Lynen Research Fellowship. F. D. acknowledges support from MCIN/AEI/10.13039/501100011033, and "FEDER, a way to make Europe," by the European Union (PID2022-138269NB-I00).

Data availability—All simulations, raw data, code to process the data, figures and data points on the figures in the main text and the Supplemental Material [21] are available from the Open Data folder accessible through the digital object identifier ("DOI") [48].

The authors declare no competing interests.

[1] M. V. Berry and M. Wilkinson, Diabolical points in the spectra of triangles, Proc. R. Soc. A **392**, 15 (1984).
[2] W. Wernsdorfer and R. Sessoli, Quantum phase interference and parity effects in magnetic molecular clusters, Science **284**, 133 (1999).
[3] R. Sessoli, D. Gatteschi, A. Caneschi, and M. A. Novak, Magnetic bistability in a metal-ion cluster, Nature (London) **365**, 141 (1993).
[4] L. Thomas, F. Lionti, R. Ballou, D. Gatteschi, R. Sessoli, and B. Barbara, Macroscopic quantum tunnelling of magnetization in a single crystal of nanomagnets, Nature (London) **383**, 145 (1996).
[5] J. von Delft and C. L. Henley, Destructive quantum interference in spin tunneling problems, Phys. Rev. Lett. **69**, 3236 (1992).
[6] D. Loss, D. P. DiVincenzo, and G. Grinstein, Suppression of tunneling by interference in half-integer-spin particles, Phys. Rev. Lett. **69**, 3232 (1992).
[7] A. Garg, Topologically quenched tunnel splitting in spin systems without Kramers' degeneracy, Europhys. Lett. **22**, 205 (1993).
[8] E. Burzurí, F. Luis, O. Montero, B. Barbara, R. Ballou, and S. Maegawa, Quantum interference oscillations of the superparamagnetic blocking in an Fe_8 molecular nanomagnet, Phys. Rev. Lett. **111**, 057201 (2013).
[9] W. Wernsdorfer, N. E. Chakov, and G. Christou, Quantum phase interference and spin-parity in Mn_{12} single-molecule magnets, Phys. Rev. Lett. **95**, 037203 (2005).
[10] Z. Scherübl, A. Pályi, G. Frank, I. Lukács, G. Fülöp, B. Fülöp, J. Nygård, K. Watanabe, T. Taniguchi, G. Zaránd, and S. Csonka, Observation of spin–orbit coupling induced Weyl points in a two-electron double quantum dot, Commun. Phys. **2**, 108 (2019).
[11] C. F. Hirjibehedin, C.-Y. Lin, A. F. Otte, M. Ternes, C. P. Lutz, B. A. Jones, and A. J. Heinrich, Large magnetic anisotropy of a single atomic spin embedded in a surface molecular network, Science **317**, 1199 (2007).
[12] F. D. Natterer, F. Donati, F. Patthey, and H. Brune, Thermal and magnetic-field stability of holmium single-atom magnets, Phys. Rev. Lett. **121**, 027201 (2018).
[13] A. Singha, P. Willke, T. Bilgeri, X. Zhang, H. Brune, F. Donati, A. J. Heinrich, and T. Choi, Engineering atomic-scale magnetic fields by dysprosium single atom magnets, Nat. Commun. **12**, 4179 (2021).
[14] S. Loth, S. Baumann, C. P. Lutz, D. M. Eigler, and A. J. Heinrich, Bistability in atomic-scale antiferromagnets, Science **335**, 196 (2012).
[15] A. Spinelli, B. Bryant, F. Delgado, J. Fernández-Rossier, and A. F. Otte, Imaging of spin waves in atomically designed nanomagnets, Nat. Mater. **13**, 782 (2014).
[16] J. Hwang, D. Krylov, R. Elbertse, S. Yoon, T. Ahn, J. Oh, L. Fang, W. Jang, F. H. Cho, A. J. Heinrich, and Y. Bae, Development of a scanning tunneling microscope for variable temperature electron spin resonance, Rev. Sci. Instrum. **93**, 093703 (2022).
[17] M. Yamada, K. Nakatsuji, and F. Komori, Nitrogen adsorption on Cu(001): Mechanisms of stress relief and coexistence of two domains, e-J. Surf. Sci. Nanotechnol. **21**, 337 (2023).
[18] C. F. Hirjibehedin, C. P. Lutz, and A. J. Heinrich, Spin coupling in engineered atomic structures, Science **312**, 1021 (2006).
[19] S. Yan, D.-J. Choi, J. A. J. Burgess, S. Rolf-Pissarczyk, and S. Loth, Control of quantum magnets by atomic exchange bias, Nat. Nanotechnol. **10**, 40 (2014).
[20] R. J. G. Elbertse, D. Coffey, J. Gobeil, and A. F. Otte, Remote detection and recording of atomic-scale spin dynamics, Commun. Phys. **3**, 94 (2020).
[21] See Supplemental Material at http://link.aps.org/supplemental/10.1103/PhysRevLett.133.166703 for an overview of experimental parameters, for additional simulations and for additional control experiments.
[22] J. Fernández-Rossier, Theory of single-spin inelastic tunneling spectroscopy, Phys. Rev. Lett. **102**, 256802 (2009),
[23] F. Delgado, J. J. Palacios, and J. Fernández-Rossier, Spin-transfer torque on a single magnetic adatom, Phys. Rev. Lett. **104**, 026601 (2010).
[24] S. Loth, M. Etzkorn, C. P. Lutz, D. M. Eigler, and A. J. Heinrich, Measurement of fast electron spin relaxation times with atomic resolution, Science **329**, 1628 (2010).
[25] S. Loth, C. P. Lutz, and A. J. Heinrich, Spin-polarized spin excitation spectroscopy, New J. Phys. **12**, 125021 (2010).
[26] J. W. Nicklas, A. Wadehra, and J. W. Wilkins, Magnetic properties of Fe chains on Cu2N/Cu(100): A density functional theory study, J. Appl. Phys. **110**, 123915 (2011).
[27] B. Bryant, A. Spinelli, J. J. T. Wagenaar, M. Gerrits, and A. F. Otte, Local control of single atom magnetocrystalline anisotropy, Phys. Rev. Lett. **111**, 127203 (2013).
[28] S. Yan, D.-J. Choi, J. A. J. Burgess, S. Rolf-Pissarczyk, and S. Loth, Three-dimensional mapping of single-atom magnetic anisotropy, Nano Lett. **15**, 1938 (2015).
[29] S. Yan, L. Malavolti, J. A. J. Burgess, A. Droghetti, A. Rubio, and S. Loth, Nonlocally sensing the magnetic states of nanoscale antiferromagnets with an atomic spin sensor, Sci. Adv. **3**, e1603137 (2017).
[30] S. Rolf-Pissarczyk, S. Yan, L. Malavolti, J. A. J. Burgess, G. McMurtrie, and S. Loth, Dynamical negative differential resistance in antiferromagnetically coupled few-atom spin chains, Phys. Rev. Lett. **119**, 217201 (2017).

[31] C. Rudowicz, K. Tadyszak, T. Ślusarski, M. Verissimo-Alves, and M. Kozanecki, Modeling spin Hamiltonian parameters for Fe^{2+} ($S = 2$) adatoms on Cu2N/Cu(100) surface using semiempirical and density functional theory approaches, Appl. Magn. Reson. **50**, 769 (2019).
[32] P. Bruno, Berry phase, topology, and degeneracies in quantum nanomagnets, Phys. Rev. Lett. **96**, 117208 (2006).
[33] R. Žitko and Th. Pruschke, Many-particle effects in adsorbed magnetic atoms with easy-axis anisotropy: The case of Fe on the CuN/Cu(100) surface, New J. Phys. **12**, 063040 (2010).
[34] S. Loth, K. von Bergmann, M. Ternes, A. F. Otte, C. P. Lutz, and A. J. Heinrich, Controlling the state of quantum spins with electric currents, Nat. Phys. **6**, 340 (2010).
[35] F. Delgado and J. Fernández-Rossier, Spin decoherence of magnetic atoms on surfaces, Prog. Surf. Sci. **92**, 40 (2017).
[36] Y. Bae, K. Yang, P. Willke, T. Choi, A. J. Heinrich, and C. P. Lutz, Enhanced quantum coherence in exchange coupled spins via singlet-triplet transitions, Sci. Adv. **4**, eaau4159 (2018).
[37] T. S. Seifert, S, Kovarik, D. M. Juraschek, N. A. Spaldin, P. Gambardella, and S. Stepanow, Longitudinal and transverse electron paramagnetic resonance in a scanning tunneling microscope, Sci. Adv. **6**, eabc5511 (2020).
[38] J. Kim, W. Jang, T. H. Bui, D.-J. Choi, C. Wolf, F. Delgado, Y. Chen, D. Krylov, S. Lee, S. Yoon, C. P. Lutz, A. J. Heinrich, and Y. Bae, Spin resonance amplitude and frequency of a single atom on a surface in a vector magnetic field, Phys. Rev. B **104**, 174408 (2021).
[39] W. Paul, K. Yang, S. Baumann, N. Romming, T. Choi, C. P. Lutz, and A. J. Heinrich, Control of the millisecond spin lifetime of an electrically probed atom, Nat. Phys. **13**, 403 (2017).
[40] H. Bethe, Zur Theorie der Metalle, Z. Phys. **71**, 205 (1931).
[41] F. Delgado, M. M. Otrokov, and A. Arnau, Spin wave excitations in low dimensional systems with large magnetic anisotropy, arXiv:2310.15942.
[42] W. Wernsdorfer, Molecular nanomagnets: Towards molecular spintronics, Int. J. Nanotechnology **7**, 497 (2010).
[43] S. Baumann, W. Paul, T. Choi, C. P. Lutz, A. Ardavan, and A. J. Heinrich, Electron paramagnetic resonance of individual atoms on a surface, Science **350**, 417 (2015).
[44] K. Yang, W. Paul, S.-H. Phark, P. Willke, Y. Bae, T. Choi, T. Esat, A. Ardavan, A. J. Heinrich, and C. P. Lutz, Coherent spin manipulation of individual atoms on a surface, Science **366**, 509 (2019).
[45] L. Marcano, I. Orue, D. Gandia, L. Gandarias, M. Weigand, R. M. Abrudan, A. García-Prieto, A. García-Arribas, A. Muela, M. L. Fdez-Gubieda, and S. Valencia, Magnetic anisotropy of individual nanomagnets embedded in biological systems determined by axi-asymmetric x-ray transmission microscopy, ACS Nano **16**, 7398 (2022).
[46] Q. A. Pankhurst, J. Connolly, S. K. Jones, and J. Dobson, Applications of magnetic nanoparticles in biomedicine, J. Phys. D **36**, R167 (2003).
[47] W. Wernsdorfer, N. E. Chakov, and G. Christou, Determination of the magnetic anisotropy axes of single-molecule magnets, Phys. Rev. B **70**, 132413 (2004).
[48] R. J. G. Elbertse, D. Borodin, J. Oh, T. Ahn, J. Hwang, J. C. Rietveld, A. J. Heinrich, F. Delgado, S. Otte, and Y. Bae, Zenodo Version 1.1 (2024), 10.5281/zenodo.12629599.